Fluorination of Graphene: A Spectroscopic and Microscopic Study
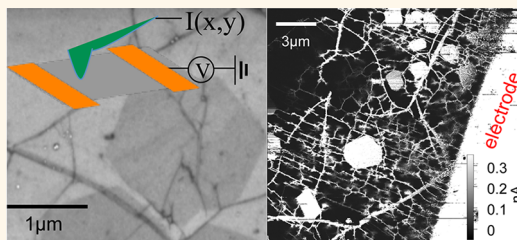
Bei Wang,[†] Junjie Wang,[†] and Jun Zhu[†,‡,*]

[†]Department of Physics and [‡]Materials Research Institute, The Pennsylvania State University, University Park, Pennsylvania 16802, United States

ABSTRACT Since the advent of graphene, there has been intense interest in exploring the possibility of incorporating fluorinated graphene (FG), an ultrathin insulator, into graphene electronics as barriers, gate dielectrics, and optoelectronic elements. Here we report on the synthesis of FG from single-layer graphene sheets grown by chemical vapor deposititon (CVD) using CF_4 plasma. We examine its properties systematically *via* microscopic and spectroscopic probes. Our studies show that, by controlling the conditions of the plasma, FG of varying fluorine coverage can be produced; however, the resulting material contains a mixture of CF_x ($x = 1-3$) bonds. Existing grain boundaries and lattice defects of CVD graphene play an important role in controlling its rate of fluorination and the damage of the sheet. Combining topography and current mapping, we demonstrate that the spatial distribution of fluorine on CVD graphene is highly inhomogeneous, where multilayer islands and structural features such as folds, wrinkles, and ripples are less fluorinated and consequently form a conductive network through which charge transport occurs. It is the properties of this network that manifest in the electrical transport of FG sheets. Our experiments reveal the many challenges of deriving electronics-quality FG from current CVD graphene while at the same time point to the possible solutions and potential of FG in graphene electronics and optoelectronics.

KEYWORDS: graphene fluoride · fluorographene · XPS · conductive AFM · chemical vapor deposition · charge transport

The discovery of graphene has led to an explosion of research activities pursing the vision of building nanoscale electronics by synthesizing, processing, and assembling intrinsically two-dimensional materials together in a bottom-up fashion. To implement the enormous range of functionalities that current electronics and optoelectronics perform, metallic, semiconducting, and insulating elements are all needed. Graphene is an excellent conductor but is not suitable for digital and optical operations due to the absence of a band gap. Chemical functionalization, for example, the formation of graphene oxide and its reduction, opens many new doors for using graphene in materials applications.[1] Electronically, chemisorbed adatoms and molecular groups create sp³-hybridized bonds, which modify the π bands of graphene and can lead to the opening of a gap at large adatom coverage. A full hydrogenation (graphane) or fluorination (graphene monofluoride) is expected to turn graphene into an insulator with a large gap greater than 6 eV,[2−5] while partially and periodically fluorinated graphene (FG) could be a semiconductor with a variable gap.[6] Fluorination has a particular appeal in this approach thanks to the vast existing knowledge of the synthetic methods and properties of fluorinated carbon.[7,8] Studies to date have shown that FG can indeed be very resistive,[6,9−12] where the charge transport exhibits hopping characteristics.[9,11−14] The drastic decrease of conductivity upon chemical functionalization is supported by quantum transport calculations.[15] Experiments have produced transparent FG with an optical gap of ~3 eV,[6,10,16] and several defect-induced photofluorescence modes in the visible range are observed in nearly stoichiometric graphene monofluoride.[17] These studies show that FG is indeed promising as the material for barrier, gate dielectric, coating, or performing optoelectronic functions in nanoelectronics based on graphene and other two-dimensional materials.

To further explore this possibility, the synthesis and properties of FG derived from large-scale synthesized graphene sheets, such as those produced by chemical vapor deposition (CVD), need to be carefully examined. Specifically, it is important to understand and control not just the density of

the C−F bonds but also the lattice damage (e.g., vacancies and line defects) in the fluorination process, which is critical to the integrity and functionality of the FG sheet. Transport and optical measurements cannot differentiate the effect of lattice damage and sp^3-hybridized fluorine. CVD-grown graphene is also far from the perfect single-crystalline sheet often assumed in calculations. Grain boundaries, lattice defects, and wrinkles and folds generated in the growth and transfer processes may significantly affect the fluorination process.[18−20] The uniformity of the fluorine coverage in FG is an important metric in its potential applications such as tunneling barriers. To examine the local fluorine density, microscopic probes are necessary. Furthermore, it would be desirable to have a fluorination method compatible with lithography to pattern areas of FG and graphene within a single sheet,[21] an example of which was demonstrated by removing fluorine selectively using electron irradiation.[12,14]

With these goals in mind, we have conducted a systematic and comprehensive study of the synthesis and properties of FG derived from CVD-grown graphene using CF_4 plasma and a wide range of spectroscopic and microscopic tools including X-ray photoelectron spectroscopy (XPS), Raman, optical absorption, electrical transport, and conductive atomic force microscopy (c-AFM). A rich tapestry of information emerged by correlating results obtained using these different probes. XPS of FG on a copper substrate shows a high degree of fluorine coverage in the range of tens of percent but also reveals the coexistence of CF_x ($x = 1−3$) bonds, indicating the presence of lattice damage. A comparison to FG produced from exfoliated graphene suggests that grain boundaries and existing lattice defects of CVD-grown graphene play an important role in controlling its fluorination and the formation of lattice damage. Furthermore, large areas of graphene film on a copper substrate are resistant to fluorination, which points to the importance of substrate interaction. Electrical transport studies show that the resistivity of the FG sheet increases with increasing fluorine coverage and can be very insulating indeed. However, c-AFM mapping indicates that the spatial distribution of fluorine is far from uniform in FG derived from CVD-grown graphene. Imperfect structural features including multilayer islands, wrinkles, folds, and ripples are *less* fluorinated, and consequently, charge conduction occurs through a network formed by these features. Macroscopic transport measurements probe the connectivity of the network, instead of the conductivity of fluorinated area. This picture departs from the simple scenario of a mixture of sp^2 and sp^3 carbon in a homogeneous FG sheet and calls for more realistic considerations in calculations and interpretations of transport and optical data on FG. The c-AFM technique employed here can be used to assess the spatial uniformity of other types of functionalized graphene

such as graphene oxide and surface modifications of other 2D materials in general.

RESULTS AND DISCUSSION

Synthesis of Graphene and FG. Graphene sheets are synthesized on 25 μm copper foil (Alpha Aesar) using a low-pressure CVD method following ref 18. As-grown sheets show an average I_D/I_G of less than 0.1. The areal percentage of multilayer islands varies from 5 to 20%. Devices made of synthesized sheet show an average field effect mobility of ∼5000 cm^2/Vs (Wang *et al.*, unpublished), indicating the high quality of the synthesized sheet. CF_4 plasma is chosen because it is fast and compatible with lithography and also because of its prior use in fluorinating nanotubes[22] and exfoliated graphene.[23,24] The process is done in a Versalock 700 ICP (Plasma-Therm) reactive ion etch chamber at room temperature. We investigated two approaches of synthesizing FG. In the first approach, CVD graphene sheets are fluorinated directly after growth on the copper substrate. In the second approach, the fluorination is done after the graphene sheet has been transferred to a quartz substrate and then annealed in a mixture of Ar/H$_2$ (90%/10%) at 450 °C for 2 h. XPS studies are performed on as-grown graphene and FG supported on the copper substrate. Raman, absorption, electrical transport, and c-AFM measurements are done on FG supported on a quartz substrate. We have conducted a plasma time sequence trial and a power sequence trial. In the time sequence, the bias power is set to $P = 10$ W and the duration of the plasma $T = 3, 10, 12, 15,$ and 20 min. In the power sequence, the duration of the plasma is set to $T = 10$ min and $P = 10, 12, 14, 15,$ and 20 W. Measurements corresponding to the same condition are performed on samples fluorinated simultaneously to minimize recipe fluctuations.

Raman Spectroscopy. Figure 1a,b shows the Raman spectra of FG derived from CVD graphene and exfoliated graphene, respectively, with plasma power $P = 10$ W and increasing duration T from 3 to 20 min (labeled as 10W3m and so on). The I_D/I_G and the strength of the Raman signals display a trend consistent with previous studies of defects (including fluorination) in sp^2 carbon.[6,10,25,26] However, the rate of fluorination on CVD and exfoliated graphene appears to be quite different. In FG synthesized from CVD graphene, $I_D/I_G \sim 1$ (2−3% defect coverage) is reached after about 3 min (magenta trace in Figure 1a), whereas similar spectra only appear after 20 min of plasma on exfoliated graphene (red trace in Figure 1b). This difference shows that CVD graphene is more chemically reactive than exfoliated graphene. We suspect that this increased reactivity originates from the defect-rich grain boundaries,[19,20] which are absent in exfoliated graphene. More evidence is presented in the XPS studies below.
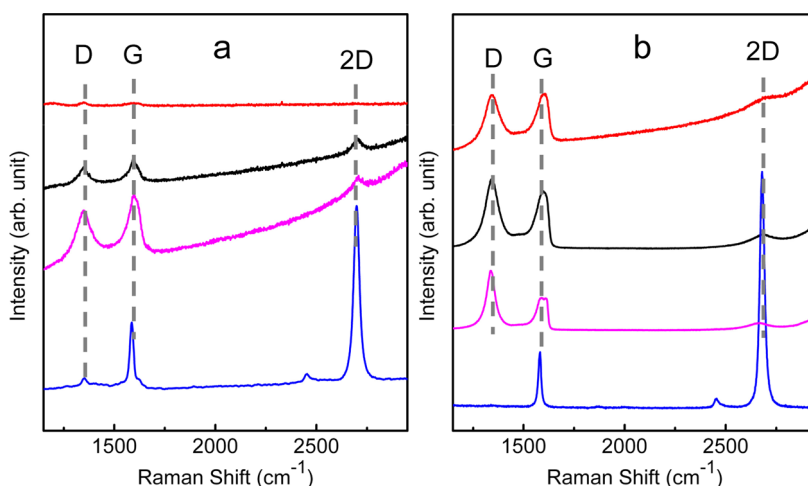
Figure 1. Raman spectra of as-grown and fluorinated graphene obtained by CVD synthesis (a) and mechanical exfoliation (b). From bottom to top: as-grown (blue), 10W3m (magenta), 10W10m (black), and 10W20m (red).

XPS. XPS is performed on FG synthesized from CVD graphene to further characterize the fluorine coverage and probe the nature of the chemical bonds. Survey and high-resolution (HR) spectra are collected on as-grown graphene and FG sheets supported on a copper substrate. Figure 2 shows the HR spectra of the C1s, F1s, and Cu2p core electron states on FG synthesized with $P = 10$ W and $T = 3, 10, 12, 15$, and 20 min, together with those of the as-grown graphene.

In as-grown graphene, the C1s spectrum exhibits a single, asymmetric peak C_0 at $E_0 = 284.3$ eV, which is the signature of sp^2 carbon, and the Cu2p peak splits into $2p_{3/2}$ and $2p_{1/2}$ due to spin-orbit coupling at binding energies of 932.5 and 952.3 eV, respectively. These energies correspond to that of elemental copper and confirm previous reports of graphene film acting as corrosion-inhibiting coating on metals.[27] No signal from fluorine is detected.

After plasma treatment, several satellite peaks (C_2–C_5 in Figure 2a) start to develop in the C1s spectra at relatively fixed binding energies. Their peak energies $\Delta E_i = E_i - E_0$ (given by the fit to the 12m spectrum) and normalized spectrum weight (area under the peak) are given in Table 1. The appearance of C_3–C_5 is accompanied by prominent peaks occurring at $E_{A'} = 687.3$ eV and $E_A = 688.3$ eV in the F1s spectrum, which we attribute to the low-coverage semi-ionic ($E_{A'}$) and high-coverage covalent (E_A) C–F bonds in fluorinated carbon, respectively.[28,29] Correspondingly, we identify C_3–C_5 with the C1s state in bulk –CF, edge –CF$_2$, and terminal –CF$_3$ bonds, respectively, using the upshifts of their binding energies from sp^2 carbon ($\Delta E_3 = 5.1$ eV, $\Delta E_4 = 7.2$ eV, and $\Delta E_5 = 9.3$ eV). These binding energies are approximately 1 eV lower than that of the corresponding CF$_x$ bonds in bulk graphite fluoride and are in excellent agreement with prior results on fluorinated surface carbon.[7,16,28,29] In stark contrast to C_3–C_5, the C_2 peak persists even in the absence of the A peak in F1s,

indicating that it is *not* of carbon–fluorine origin. Its binding energy ($\Delta E_2 = 4.1$ eV) suggests C(O)O passivation of a terminal carbon atom,[31,32] which presumably occurs when an uncapped terminal carbon reacts with the air outside the plasma chamber. Lastly, a relatively broad peak C_1 centered at $\Delta E_1 = 2.7$ eV accounts for the spectrum weight between C_2 and C_0. This binding energy is consistent with secondary C*–CF$_x$ ($x = 1$–3) atoms[30] and also possible C=O bonds formed at the external edges of platelets or internal edges of voids.[31,32] The presence of CF$_2$, CF$_3$, and possibly C(O)O and C=O bonds indicates lattice damage in the form of vacancy, void, terminal carbon, and fragmentation of the sheet in the fluorination process, as Figure 3 schematically shows. We also observe the onset of a second peak (labeled B) at $E_B = 684.4$ eV in the F1s spectra after 10 min of plasma treatment. This peak correlates with the onset of a series of higher energy satellite peaks (arrows in Figure 2c) in the Cu2p$_{1/2}$ and 2p$_{3/2}$ spectra, indicating the formation of CuF$_2$.[33] This suggests that the graphene barrier becomes permeable to fluorine after 10 min, probably due to the damage to the lattice. FG on copper appears to be more insulating as shown in the SEM images in Figure S1 of the Supporting Information.

Following the evolution of C_2–C_5 and F_{A-B} quantitatively with increasing plasma duration T (Figure 2 and Table 1) reveals many insights into the fluorination process. As Table 1 shows, the plasma treatment of CVD graphene produces all three types of CF$_x$ ($x = 1$–3) bonds, and the percentage of each type increases with increasing T initially, yielding a total of 28% fluorinated carbon atoms at $T = 12$ min. However, CF bonds only account for about one-half of the fluorinated carbon. In another word, FG synthesized from CVD graphene is quite defective. In comparison, Raman studies on FG synthesized from exfoliated graphene (see Figure 1b) show much less fluorine coverage under comparable
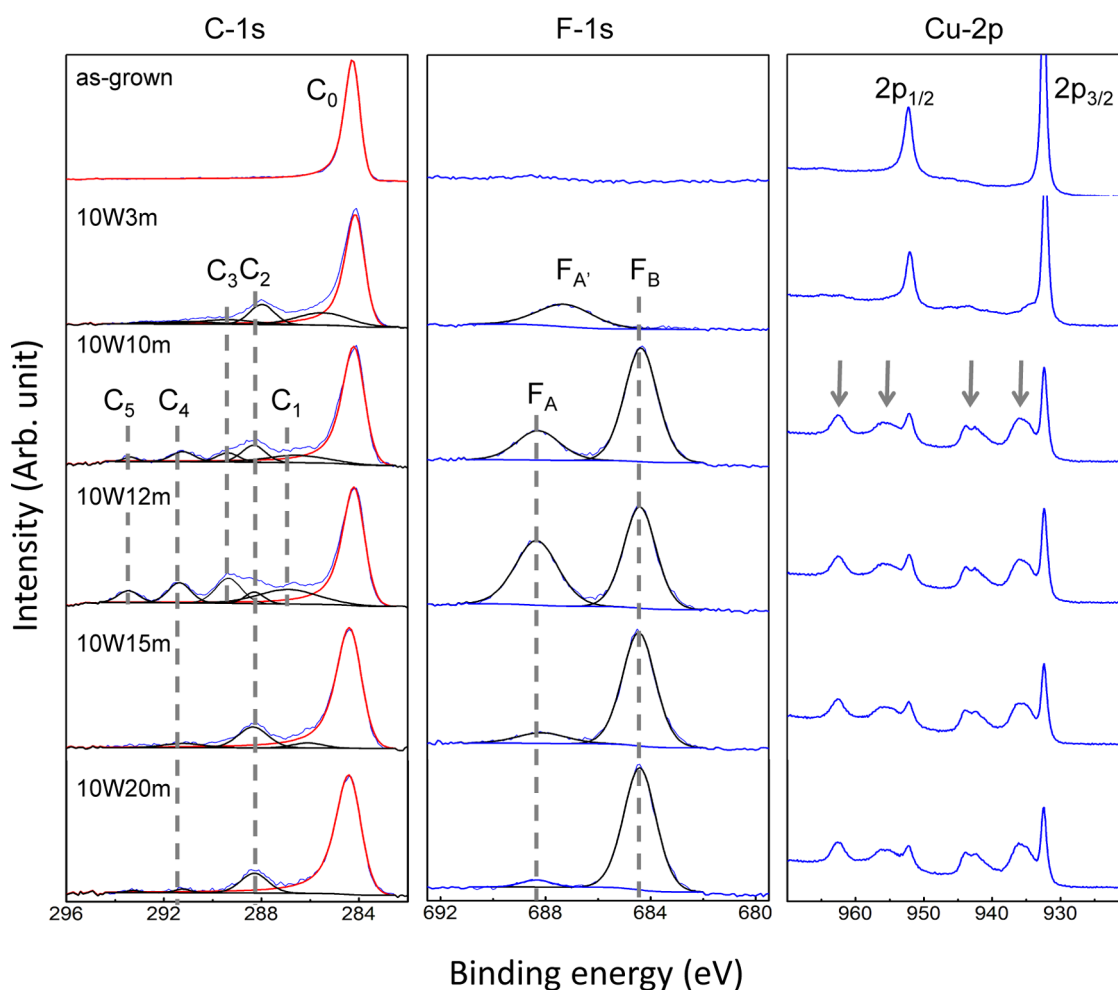
Figure 2. High-resolution XPS spectra of C1s, F1s, and Cu2p states on as-grown and fluorinated CVD graphene. The plasma conditions are indicated in the plot. The C1s spectra are scaled to have C_0 peaks of the same height. The F1s and Cu2p spectra are plotted as taken.

TABLE 1. Energy and Spectrum Weight of the C1s Bonding States in As-Grown and Fluorinated CVD Graphene

		C_0	C_2	C_3	C_4	C_5	C_1	
		C—C	C(0)O	CF	CF_2	CF_3	other	
$\Delta E_i =$								CF +
$E_i - E_0$ (eV)		0	4.1	5.1	7.2	9.3	2.7	$CF_2 + CF_3$
normalized spectrum	0	0	100	0	0	0	0	0
weight (%)	3 min	56.7	13.6	6.9	3.8	0.8	18.2	11.5
	10 min	64.9	10.5	5.3	6.0	1.6	11.7	12.9
	12 min	50.1	4.6	13.1	9.3	5.1	17.8	27.5
	15 min	74.8	16.3	0	4.8	0	4.1	4.8
	20 min	81.8	15.5	0	1.7	1.0	0	1.7

Figure 3. Examples of chemical bonds in FG synthesized from CVD graphene.

conditions, and most importantly, more than 90% of the CF bonds are reversible upon thermal annealing, indicating also much less lattice damage (see Figure S2 of the Supporting Information for details). A possible explanation is that, in CVD-grown graphene, the defective lattice sites at the grain boundaries are more chemically active,[19,20] and this leads to a faster reaction, but also more lattice damage, signaled by the
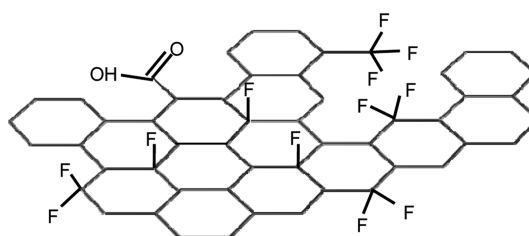
formation of CF_2 and CF_3 bonds. Lattice damage limits the potential application of FG as tunnel barriers or dielectric layers in electronics because of leakage problems. However, our studies of FG synthesized from exfoliated graphene suggest that this challenge can be overcome by using graphene with large grain sizes, the growth of which has been demonstrated.[34]

The C1s and F1s spectra beyond 12 min reveal another interesting aspect of fluorinating graphene on a copper substrate. From 12 to 20 min, we observe a sharp loss of total carbon count by 50%; meanwhile, the weight of the CF_x and the F_A peaks continues to
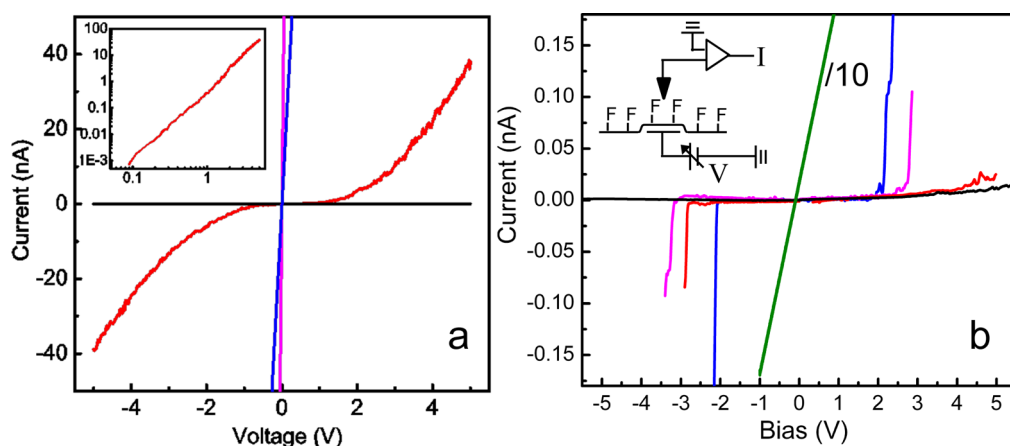
Figure 4. (a) Typical *IV* curves of fluorinated CVD graphene devices. *P* = 10 W and *T* = 3 (magenta), 10 (blue), 12 (red), and 15 (black) min. The zero-bias resistance *R* is 1 MΩ, 5.3 MΩ, 3 GΩ, and >280 GΩ, respectively. The inset shows the *IV* of the 12 min device in a log−log plot showing power law dependence $I = V^{\alpha}$. The exponent α = 2.65 here. (b) Tunneling current *vs* bias voltage with the AFM tip contacting a bilayer island on as-grown (olive, current divided by 10), 10W3m (blue), 10W10m (magenta), 10W12m (red), and 10W15m (black) devices. Inset: Schematic diagram of the measurement circuit.

vanish, and the remaining carbon is mostly sp^2 bonded. These observations suggest continuous removal of carbon atoms from fragmented sp^2 graphene nanoplatelets in the plasma chamber, whose edges are subsequently passivated in air by C(O)O bonds as indicated by the large C$_2$ component. This scenario is contrary to a continuous conversion of sp^2 carbon to carbon−fluorine bonds observed in suspended graphene.[6] Multilayer islands are more resistant to fluorination (see c-AFM results below), but the area is too small (up to 20%) to account for the spectrum weight of the C$_0$ peak, which is ∼80%, in the bottom two panels in Figure 2. The trend shown here also appears in samples progressively fluorinated by increasing the plasma power instead of duration (see Figure S3 of the Supporting Information for the power sequence).

Comparison to FG synthesized on a quartz substrate points to the inhibiting role of copper substrate. UV−Vis−NIR absorption studies of FG on quartz obtained after 15 min of plasma treatment show absorbance less than 10% of pristine graphene, which suggests a low fraction of intact sp^2 carbon area (see Figure S4 of the Supporting Information for more details). Indeed, a recent study shows that fluorine chemisorbs to high-index Cu facets preferentially, which suggests that the fluorine-resistant graphene patches observed here are grown on low-index Cu facets.[35] In order to synthesize uniform FG suitable for a "fluorinate before transfer" approach, a better understanding and control of the effect of the copper substrate is necessary.

In the second half of the paper, we investigate the electrical transport properties of FG using two-terminal conductance and c-AFM measurements. Titanium electrodes (35 nm thick) are deposited on FG sheets fluorinated on quartz using a stencil mask. A typical sample has five electrodes in parallel with the dimensions of the graphene sheet straddled between two adjacent electrodes being approximately 4 mm (width) × 1 mm (length). Two-terminal *IV* measurements are performed by sweeping the drain-source bias V_{ds} and recording the current I_{ds} between adjacent electrodes using a Keithley 6430 DC sourcemeter.

Conductance of FG. Figure 4a shows typical *IV* curves of FG synthesized on quartz using *P* = 10 W and *T* = 3, 10, 12, and 15 min. Measurements from many devices show that the *IV* is linear with a resistance *R* of ∼1 MΩ and several MΩ for *T* = 3 and 10 min. Above 10 min, the *IV* becomes nonlinear with large low-bias resistance *R*. The variation among devices also increases. *R* ranges from GΩ to hundreds of GΩ for 12 min devices and is more than the parasitic resistance of our measurement setup (∼280 GΩ) for 15 min devices. Using the XPS data as a rough guide, we observe resistance increases of more than 7 orders of magnitude from 10 kΩ to greater than 100 GΩ as the fluorine coverage increases from zero to a few tens of percent. This observation is in good agreement with prior studies conducted on FG synthesized using XeF$_2$[6,10] or exfoliated from bulk graphite fluoride.[9,11,12] Despite the similar resistance range observed in macroscopic measurements, c-AFM measurements described below reveal unique microscopic aspects of conduction in FG synthesized from CVD graphene.

Conductive AFM. Current maps are obtained by measuring the current flow from one electrode to the AFM tip using a current preamplifier integrated on the tip (Asylum Research MFP-3D with ORCA module). Scanning away from the contact, the current map traces out the paths of current flow directly. Figure 5a shows a local area on a 10W3m device. Remarkably, although *IV* curves on this device show an ohmic resistance of ∼1 MΩ, the current flow through the sheet is not uniform but rather follows a network formed by structural
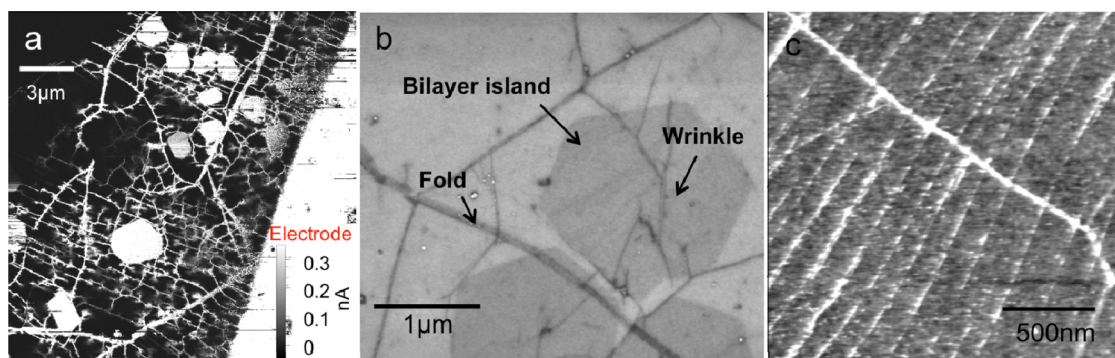
Figure 5. (a) c-AFM current map of a device made with 10W3m fluorinated CVD graphene on quartz. The bright area at the lower right corner is the electrode. (b) SEM image of as-grown graphene transferred to a SiO_2/Si substrate. Examples of various features are labeled in the image following common nomenclatures. (c) AFM image of another transferred graphene sheet. The fine ripples are outlined by residual polymer contaminant and are difficult to see otherwise.
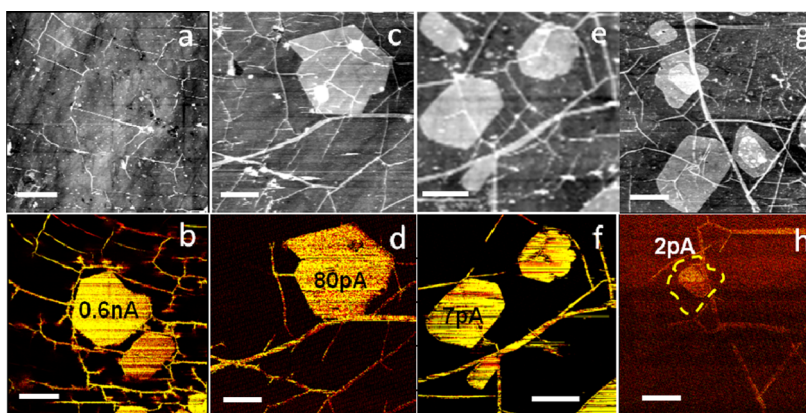

Figure 6. AFM topographic (top row) and current (bottom row) mapping on fluorinated graphene devices. From left to right: 10W3m (a,b), 10W10m (c,d), 10W12 m (e,f), and 10W15 m (g,h). The voltage bias is 3.5 V in (b) and 5 V in (d), (f), and (h). In (b−h), the typical current level is labeled for when the AFM tip is above the respective multilayer islands. The bilayer islands are difficult to see in (a) due to the rough quartz surface but are clearly outlined in (b). The height of fluorinated graphene sheets increases to a few nanometers, and the multilayer islands are clearly visible in (c), (e), and (g). The scale bar is 1 μm in all images. Images are taken 5−10 μm away from electrode.

features commonly seen in CVD-grown graphene such as bilayer islands, folds (2-layer height, width ∼100 nm), wrinkles (line width <50 nm), and ripples (fine parallel lines with spacing ∼150 nm).[18,36] Figure 5b,c shows SEM and AFM images of these features in our as-grown graphene. The current flow pattern indicates that these structures are less fluorinated than the flat area of the sheet. This is the first observation of inhomogeneous electrical transport through fluorinated graphene. It is perhaps not surprising given that the underlayers of bilayer islands and folds are protected from the directional plasma by the top layer, and C−F bonds may be difficult to form on the side of wrinkles and ripples because of the negative curvature.[37]

The correlation between morphology and conduction and the evolution of this conductive network with increasing fluorine coverage are further illustrated in Figure 6a−h, where we show simultaneously the AFM topographic and current maps of the same areas on FG devices fluorinated with increasing plasma duration T from 3 to 15 min. As the fluorination progresses, fine ripples and wrinkles first turn dark in the current map, followed by large wrinkles and folds. As T increases, bilayer islands also disappear in the current map, probably due to a combination of fluorination and loss of connectivity to the network. In Figure 6h, an island containing both bilayer and trilayer regions only shows conduction in the trilayer region, suggesting that the two top layers have been fluorinated. This vertical progression may result from the lattice damage discussed in the XPS section. The typical current measured decreases rapidly with increasing T. For example, as T increases from 10 to 12 min from (d) to (f), the current drops by an order of magnitude from 80 to 7 pA. This is consistent with our IV data, where the two-terminal resistance of a macroscopic device increases quickly from several MΩ to more than GΩ between T = 10 and 12 min. These c-AFM studies show that the fluorine coverage in FG synthesized using CVD graphene is highly inhomogeneous due to the existence of multilayer islands, folds, wrinkles, and ripples in as-grown and transferred samples. These structures are less fluorinated and consequently form the conductive

network through which charge transport preferentially occurs. Macroscopic transport characteristics, such as resistance and *IV*, probe the properties of this network, instead of the bulk conductivity of FG. This is probably not the case in FG obtained from bulk graphite fluoride,[9,11,12] where folds and wrinkles are much less likely. The nonuniform fluorine coverage of FG synthesized from CVD graphene is undesirable to its potential applications as dielectric films and tunnel barriers. There are, however, a number of ways to improve the synthesis[38,39] and transfer[40] of graphene to address this issue. For example, a H_2 etching step can eliminate the growth of multilayer islands[38,39] while a redeposition of polymer reduces the formation of wrinkles and cracks in transferred graphene.[40]

On the other hand, a controlled fluorination of the top layer of a bilayer graphene sheet offers a facile and transfer-free approach to create an insulator/graphene junction,[41] which may be a useful component in 2D layered electronics. To explore this idea, we perform local tunneling measurements on fluorinated bilayer islands. Point *IV* spectra are taken by positioning the AFM tip in contact above a bilayer island and measure the *IV* curve using a Keithley 6430 DC sub-fA sourcemeter. A schematic of the setup is shown in the inset of Figure 4b. In this configuration, the bottom layer is less fluorinated and serves as the bottom contact for the top layer, and the bilayer is chosen to be very close to, and well connected to, an electrode by folds and wrinkles to minimize the resistance of the bottom contact. Figure 4b shows representative *IV* curves from bilayer islands fluorinated for $T = 3, 10, 12,$ and 15 min. All traces exhibit strong nonlinearity and sharp onset of conduction beyond a threshold voltage V_{th}, where $V_{th} \sim 1.8-2.1$ and $2.7-3.3$ V for $T = 3$ and 10 min, respectively, and is beyond 3.5 V for $T > 10$ min. In stark contrast, two-terminal *IV* measurements on 3m and 10m devices show linear *IV* and moderate resistance

in the range of MΩ. This difference again highlights the different aspects of the FG probed in these measurements. While two-terminal *IV* measures the resistance of the conductive network, the point *IV* shown here is presumably dominated by the tunneling process through the fluorinated top layer. The increase of V_{th} with increasing T is consistent with the increased fluorine coverage of the top layer. A quantitative analysis of the point *IV* spectra is difficult because of the nonstoichiometric nature of the FG and unknown parameters of the setup. Nonetheless, these results do point to the potential of FG as integrated, ultrathin tunnel barriers in graphene circuits, and more studies need to be done to further understand and explore this venue of applications.

CONCLUSIONS

To summarize, we have synthesized fluorinated graphene from CVD-grown graphene and investigated its chemical, electrical, and optical properties using microscopic and spectroscopic probes. Our studies highlight two important practical issues in the synthesis of FG: homogeneity and defect creation, both of which are critical to its proposed applications in electronics. We show that the spatial distribution of fluorine on CVD-grown graphene strongly correlates with imperfect structural features produced in the growth and transfer steps. Consequently, the resistivity of FG is spatially nonuniform. Our results also point to the defect-rich grain boundaries of CVD-grown graphene as the source of increased chemical reactivity and lattice damage. Our experiments delineated a realistic and complex scenario of graphene fluorination and identified several challenges to the production of electronics-grade FG. Improving the synthesis and processing of graphene is key to addressing many of the challenges.

METHODS

CF₄ plasma fluorination is done in a Versalock700 ICP (Plasma-Therm) reactive ion etch chamber using gaseous CF_4 at room temperature. The gas pressure and flow rate are set to be 100 mTorr and 25 sccm, respectively. We vary the bias power P and the duration of the plasma T. The inductively coupled coil is not used.

XPS studies are performed on a Kratos Analytical Axis Ultra system using a monochromated Al Kα line. The analysis is performed with CASA XPS analysis package. The sp^2 carbon peak in the C1s spectra is fit to the Gelius function, which includes the high-energy tail arising from the vibrational modes of the lattice. The background of all spectra is computed with the Shirley algorithm. The peaks are fit to a mixed Gaussian and Lorentzian line shape.[42]

Raman spectroscopy is performed using a Renishaw inVia micro-Raman system with an excitation energy (wavelength) of 2.41 eV (514 nm) and a spot size of ~ 1 μm. The laser power is limited to below 1mW/μm² to avoid damaging samples. Each spectrum is integrated for 60 s. At least three

spectra from different spots are taken on each sample and averaged.

Absorption spectroscopy is performed using the transmission setup of Lambda 950 (PerkinElmer) in the spectrum range of 1.44 to 6 eV with a spot size of 1×3 mm². Transmission spectra of the bare quartz substrate and of the substrate with the specimen are collected, from which we calculate the absorption of the specimen using the method described in ref 43.

Conflict of Interest: The authors declare no competing financial interest.

Supporting Information Available: Comparison of as-grown and fluorinated graphene on copper. Reversibility of fluorination

on exfoliated graphene. XPS spectra of plasma fluorinated CVD graphene in a power sequence. The absorbance of fluorinated CVD graphene. This material is available free of charge *via* the Internet at http://pubs.acs.org.

REFERENCES AND NOTES

1. Zhu, Y. W.; Murali, S.; Cai, W. W.; Li, X. S.; Suk, J. W.; Potts, J. R.; Ruoff, R. S. Graphene and Graphene Oxide: Synthesis, Properties, and Applications. *Adv. Mater.* **2010**, *22*, 3906–3924.

2. Sofo, J. O.; Chaudhari, A. S.; Barber, G. D. Graphane: A Two-Dimensional Hydrocarbon. *Phys. Rev. B* **2007**, *75*, 153401.

3. Charlier, J. C.; Gonze, X.; Michenaud, J. P. First-Principles Study of Graphite Monofluoride (CF)*n*. *Phys. Rev. B* **1993**, *47*, 16162.

4. Klintenberg, M.; Lebegue, S.; Katsnelson, M. I.; Eriksson, O. Theoretical Analysis of the Chemical Bonding and Electronic Structure of Graphene Interacting with Group IA and Group VIIA Elements. *Phys. Rev. B* **2010**, *81*, 085433.

5. Leenaerts, O.; Peelaers, H.; Hernandez-Nieves, B.; Partoens, B.; Peeters, F. First-Principles Investigation of Graphene Fluoride and Graphane. *Phys. Rev. B* **2010**, *82*, 195436.

6. Robinson, J. T.; Burgess, J. S.; Junkermeier, C. E.; Badescu, S. C.; Reinecke, T. L.; Perkins, F. K.; Zalalutdniov, M. K.; Baldwin, J. W.; Culbertson, J. C.; Sheehan, P. E.; *et al.* Properties of Fluorinated Graphene Films. *Nano Lett.* **2010**, *10*, 3001–3005.

7. Kita, Y.; Watanabe, N.; Fujii, Y. Chemical Composition and Crystal Structure of Graphite Fluoride. *J. Am. Chem. Soc.* **1979**, *101*, 3832–3841.

8. Touhara, H.; Okino, F. Property Control of Carbon Materials by Fluorination. *Carbon* **2000**, *38*, 241–267.

9. Cheng, S. H.; Zou, K.; Okino, F.; Gutierrez, H.; Gupta, A.; Shen, N.; Eklund, P.; Sofo, J.; Zhu, J. Reversible Fluorination of Graphene: Evidence of a Two-Dimensional Wide Bandgap Semiconductor. *Phys. Rev. B* **2010**, *81*, 205435.

10. Nair, R. R.; Ren, W. C.; Jalil, R.; Riaz, I.; Kravets, V. G.; Britnell, L.; Blake, P.; Schedin, F.; Mayorov, A. S.; Yuan, S. J.; *et al.* Fluorographene: A Two-Dimensional Counterpart of Teflon. *Small* **2010**, *6*, 2877–2884.

11. Withers, F.; Russo, S.; Dubois, M.; Craciun, M. Tuning the Electronic Transport Properties of Graphene through Functionalisation with Fluorine. *Nanoscale Res. Lett.* **2011**, *6*, 526.

12. Martins, S.; Withers, F.; Dubois, M.; Craciun, M. F.; Russo, S. Tuning the Transport Gap of Functionalized Graphene *via* Electron Beam Irradiation. *New J. Phys.* **2013**, *15*, 033024.

13. Withers, F.; Dubois, M.; Savchenko, A. K. Electron Properties of Fluorinated Single-Layer Graphene Transistors. *Phys. Rev. B* **2010**, *82*, 073403.

14. Withers, F.; Bointon, T. H.; Dubois, M.; Russo, S.; Craciun, M. F. Nanopatterning of Fluorinated Graphene by Electron Beam Irradiation. *Nano Lett.* **2011**, *11*, 3912–3916.

15. Roche, S.; Leconte, N.; Ortmann, F.; Lherbier, A.; Soriano, D.; Charlier, J.-C. QuantumTransport in Disordered Graphene: A Theoretical Perspective. *Solid State Commun.* **2012**, *152*, 1404–1410.

16. Jeon, K.-J.; Lee, Z.; Pollak, E.; Moreschini, L.; Bostwick, A.; Park, C.-M.; Mendelsberg, R.; Radmilovic, V.; Kostecki, R.; Richardson, T. J.; *et al.* Fluorographene: A Wide Bandgap Semiconductor with Ultraviolet Luminescence. *ACS Nano* **2011**, *5*, 1042–1046.

17. Wang, B.; Sparks, J. R.; Gutierrez, H. R.; Okino, F.; Hao, Q.; Tang, Y.; Crespi, V. H.; Sofo, J. O.; Zhu, J. Photoluminescence from Nanocrystalline Graphite Monofluoride. *Appl. Phys. Lett.* **2010**, *97*, 141915.

18. Li, X. S.; Cai, W. W.; An, J. H.; Kim, S.; Nah, J.; Yang, D. X.; Piner, R.; Velamakanni, A.; Jung, I.; Tutuc, E.; *et al.* Large-Area Synthesis of High-Quality and Uniform Graphene Films on Copper Foils. *Science* **2009**, *324*, 1312–1314.

19. Huang, P. Y.; Ruiz-Vargas, C. S.; van der Zande, A. M.; Whitney, W. S.; Levendorf, M. P.; Kevek, J. W.; Garg, S.; Alden, J. S.; Hustedt, C. J.; Zhu, Y.; *et al.* Grains and Grain Boundaries in Single-Layer Graphene Atomic Patchwork Quilts. *Nature* **2011**, *469*, 389–393.

20. Kim, K.; Lee, Z.; Regan, W.; Kisielowski, C.; Crommie, M. F.; Zettl, A. Grain Boundary Mapping in Polycrystalline Graphene. *ACS Nano* **2011**, *5*, 2142–2146.

21. Shen, N.; Sofo, J. O. Dispersion of Edge States and Quantum Confinement of Electrons in Graphene Channels Drawn on Graphene Fluoride. *Phys. Rev. B* **2011**, *83*, 245424.

22. Shoda, K.; Kohno, H.; Kobayashi, Y.; Takagi, D.; Takeda, S. Feasibility Study for Sidewall Fluorination of SWCNTs in CF_4 Plasma. *J. Appl. Phys.* **2008**, *104*, 113529.

23. Hong, X.; Cheng, S. H.; Herding, C.; Zhu, J. Colossal Negative Magnetoresistance in Dilute Fluorinated Graphene. *Phys. Rev. B* **2011**, *83*, 085410.

24. Hong, X.; Zou, K.; Wang, B.; Cheng, S. H.; Zhu, J. Evidence for Spin-Flip Scattering and Local Moments in Dilute Fluorinated Graphene. *Phys. Rev. Lett.* **2012**, *108*, 226602.

25. Ferrari, A.; Robertson, J. Interpretation of Raman Spectra of Disordered and Amorphous Carbon. *Phys. Rev. B* **2000**, *61*, 14095–14107.

26. Lucchese, M. M.; Stavale, F.; Ferreira, E. H. M.; Vilani, C.; Moutinho, M. V. O.; Capaz, R. B.; Achete, C. A.; Jorio, A. Quantifying Ion-Induced Defects and Raman Relaxation Length in Graphene. *Carbon* **2010**, *48*, 1592–1597.

27. Prasai, D.; Tuberquia, J. C.; Harl, R. R.; Jennings, G. K.; Bolotin, K. I. Graphene: Corrosion-Inhibiting Coating. *ACS Nano* **2012**, *6*, 1102–1108.

28. Bittencourt, C.; Van Lier, G.; Ke, X.; Suarez-Martinez, I.; Felten, A.; Ghijsen, J.; Van Tendeloo, G.; Ewels, C. Spectroscopy and Defect Identification for Fluorinated Carbon Nanotubes. *ChemPhysChem* **2009**, *10*, 920–925.

29. Tressaud, A.; Durand, E.; Labrugre, C.; Kharitonov, A. P.; Kharitonova, L. N. Modification of Surface Properties of Carbon-Based and Polymeric Materials through Fluorination Routes: From Fundamental Research to Industrial Applications. *J. Fluorine Chem.* **2007**, *128*, 378–391.

30. Nanse, G.; Papirer, E.; Fioux, P.; Moguet, F.; Tressaud, A. Fluorination of Carbon Blacks: An X-ray Photoelectron Spectroscopy Study 0.1. A Literature Review of XPS Studies of Fluorinated Carbons. XPS Investigation of Some Reference Compounds. *Carbon* **1997**, *35*, 175–194.

31. Stankovich, S.; Dikin, D. A.; Piner, R. D.; Kohlhaas, K. A.; Kleinhammes, A.; Jia, Y.; Wu, Y.; Nguyen, S. T.; Ruoff, R. S. Synthesis of Graphene-Based Nanosheets *via* Chemical Reduction of Exfoliated Graphite Oxide. *Carbon* **2007**, *45*, 1558–1565.

32. Dreyer, D. R.; Park, S.; Bielawski, C. W.; Ruoff, R. S. The Chemistry of Graphene Oxide. *Chem. Soc. Rev.* **2010**, *39*, 228–240.

33. Qiu, S.; Yarmoff, J. Self-Limiting Growth of Transition-Metal Fluoride Films from the Reaction with XeF_2. *Phys. Rev. B* **2001**, *63*, 115409.

34. Li, X.; Magnuson, C. W.; Venugopal, A.; Tromp, R. M.; Hannon, J. B.; Vogel, E. M.; Colombo, L.; Ruoff, R. S. Large-Area Graphene Single Crystals Grown by Low-Pressure Chemical Vapor Deposition of Methane on Copper. *J. Am. Chem. Soc.* **2011**, *133*, 2816–2819.

35. Wood, J. D.; Schmucker, S. W.; Raasch, R. T.; Doidge, G. P.; Nienhaus, L.; Damhorst, G. L.; Lyons, A. S.; Gruebele, M.; Bashir, R.; Pop, E.; Lyding, J. W. Improved Graphene Growth and Fluorination on Cu with Clean Transfer to Surfaces, 12th IEEE Conference on Nanotechnology, **2012**.

36. Ni, G. X.; Zheng, Y.; Bae, S.; Kim, H. R.; Pachoud, A.; Kim, Y. S.; Tan, C. L.; Im, D.; Ahn, J. H.; Hong, B. H. Quasi-Periodic Nanoripples in Graphene Grown by Chemical Vapor Deposition and Its Impact on Charge Transport. *ACS Nano* **2012**, *6*, 1158–1164.

37. Zhang, W.; Dubois, M.; Guerin, K.; Bonnet, P.; Kharbache, H. Effect of Curvature on C−F Bonding in Fluorinated Carbons: From Fullerene and Derivatives to Graphite. *Phys. Chem. Chem. Phys.* **2010**, *12*, 1388–1398.

38. Vlassiouk, I.; Regmi, M.; Fulvio, P.; Dai, S.; Datskos, P.; Eres, G.; Smirnov, S. Role of Hydrogen in Chemical Vapor

Deposition Growth of Large Single-Crystal Graphene. *ACS Nano* **2011**, *5*, 6069–6076.

39. Han, Z.; Kimouche, A.; Allain, A.; Arjmandi-Tash, H.; Reserbat-Plantey, A.; Pairis, S.; Reita, V.; Bendiab, N.; Coraux, J.; Bouchiat, V. Suppression of Multilayer Graphene Patches during CVD Graphene Growth on Copper. *arXiv:1205.1337* **2012**.

40. Kang, J.; Shin, D.; Bae, S.; Hong, B. Graphene Transfer: Key for Applications. *Nanoscale* **2012**, *4*, 5527–5537.

41. Britnell, L.; Gorbachev, R.; Jalil, R.; Belle, B.; Schedin, F.; Mishchenko, A.; Georgiou, T.; Katsnelson, M.; Eaves, L.; Morozov, S. Field-Effect Tunneling Transistor Based on Vertical Graphene Heterostructures. *Science* **2012**, *335*, 947–950.

42. http://www.casaxps.com/.

43. Mak, K. F.; Sfeir, M. Y.; Wu, Y.; Lui, C. H.; Misewich, J. A.; Heinz, T. F. Measurement of the Optical Conductivity of Graphene. *Phys. Rev. Lett.* **2008**, *101*, 196405.